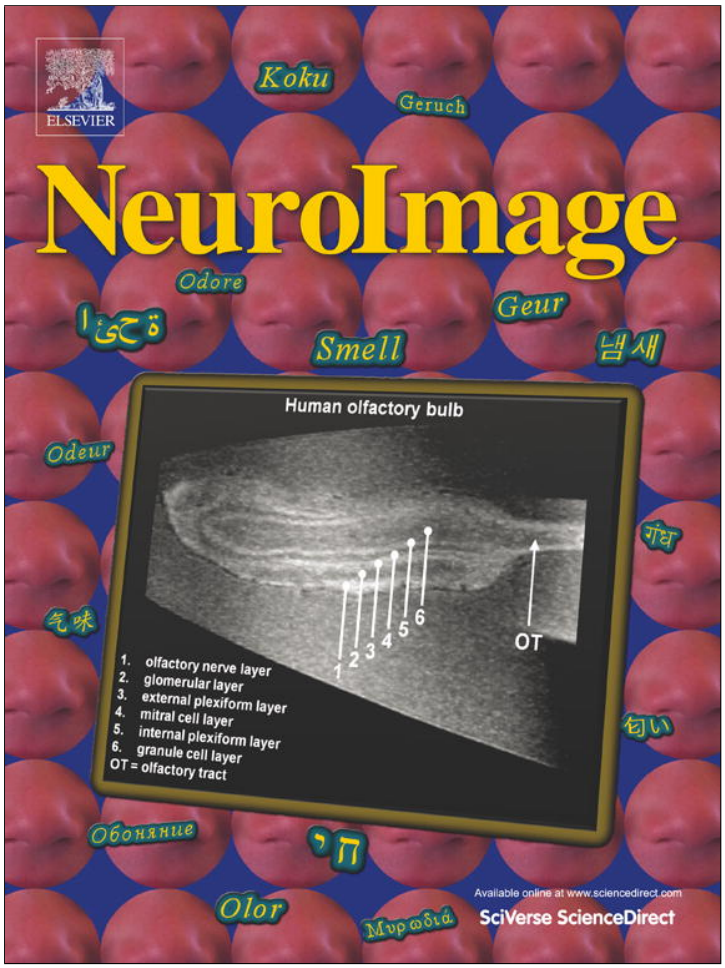

(This is a sample cover image for this issue. The actual cover is not yet available at this time.)

NeuroImage 67 (2013) 89–100

Contents lists available at SciVerse ScienceDirect

NeuroImage

journal homepage: www.elsevier.com/locate/ynimg

Parallel motion signals to the medial and lateral motion areas V6 and MT+

Sabrina Pitzalis [a,b], Chiara Bozzacchi [a], Alessandro Bultrini [a], Patrizia Fattori [c], Claudio Galletti [c], Francesco Di Russo [a,b,*]

[a] Dept. of Education for Motor Activity and Sport, University of Roma "Foro Italico", Roma, Italy
[b] Laboratory of Neuropsychology, IRCCS Santa Lucia Foundation, Roma, Italy
[c] Dept. of Human and General Physiology and Dept. of Pharmacy and Biotechnology, University of Bologna, Bologna, Italy

ARTICLE INFO

Article history:
Accepted 17 November 2012
Available online 24 November 2012

Keywords:
VEP/fMRI combination
Visual perception
Visual areas
Self motion
Spatiotemporal brain mapping
Retinotopy

ABSTRACT

MT+ and V6 are key motion areas of the dorsal visual stream in both macaque and human brains. In the present study, we combined electrophysiological and neuroimaging methods (including retinotopic brain mapping) to find the electrophysiological correlates of V6 and to define its temporal relationship with the activity observed in MT+. We also determined the spatio-temporal profile of the motion coherency effect on visual evoked potentials (VEPs), and localized its neural generators. We found that area V6 participates in the very early phase of the coherent motion processing and that its electroencephalographic activity is almost simultaneous with that of MT+. We also found a late second activity in V6 that we interpret as a re-entrant feedback from extrastriate visual areas (e.g. area V3A). Three main cortical sources were differently modulated by the motion coherence: while V6 and MT+ showed a preference for the coherent motion, area V3A preferred the random condition. The response timing of these cortical sources indicates that motion signals flow in parallel from the occipital pole to the medial and lateral motion areas V6 and MT+, suggesting the view of a differential functional role.

Introduction

In the primate visual system, motion is processed along a specialized pathway that begins in striate cortex (V1), extends through several extrastriate areas, and terminates in higher areas of the parietal and temporal lobes. Lateral areas V5/MT and MST are classically considered the key motion regions of the dorsal visual stream, being responsive to visual stimuli in motion and showing selectivity for the direction (e.g., Morrone et al., 2000; Smith et al., 2006; Tootell et al., 1995) and speed (e.g., Lebranchu et al., 2010; McKeefry et al., 2008; Pitzalis et al., 2012) of movement. Recent studies from our group have revealed the presence in the human dorsal stream of another key motion region, area V6, located medially in the parieto-occipital sulcus (Pitzalis et al., 2010). While lateral areas V5/MT and MST have been widely investigated and their role in motion processing is well grounded, the discovery of the medial motion area V6 is relatively recent and its functional role is still unknown. Human V6 has retinotopic organization, position, and neighboring relations similar to those of macaque area V6 (Galletti et al., 1999; Pitzalis et al., 2006). As in non-human primates, the human V6 is a motion area very sensitive to translational motion (Pitzalis et al., 2010; Sdoia et al., 2009), with a selective preference for fast speed of motion (Pitzalis et al., 2012), and a strong preference for coherent motion (Cardin and Smith, 2010; Helfrich et al., in press; Pitzalis et al., 2010; von Pföstl et al., 2009). Human V6 is also highly sensitive to flow fields (Cardin and Smith, 2010, 2011; Pitzalis et al., 2010) which is probably the most important visual cue for the perception of self-motion or 'egomotion' (i.e. the sensation to be moving in space).

Though motion perception in humans has been extensively studied with electrophysiological methods (e.g., see Kuba et al., 2007 for review), the effect of coherent visual motion has been less investigated. Two magnetoencephalographic (MEG) studies (Holliday and Meese, 2005; Wiest et al., 2001) found a consistent contribution of the lateral MT complex without reporting any electromagnetic activity in the medial parieto-occipital sulcus (POs). Another couple of MEG studies (Vanni et al., 2001; von Pföstl et al., 2009) suggested that the response in a medial parieto-occipital region, likely corresponding to human V6, occurred very early, with about the same latency as in V1. In contrast, a quite late activity (around 200 ms) has been reported in the same medial regions by other MEG (Urakawa et al., 2010), event-related potentials (ERP) (Mercier et al., 2009) and combined ERP/fMRI studies (Pitzalis et al., 2012). However, due to the low spatial resolution of the MEG data, past studies of this type could include in their maps some neighboring regions besides V6. Moreover, the response timing of area V6 in all these previous studies was evoked by visual stimuli that were not ideal to functionally activate V6, either for the type of the stimulus or for its size.

* Corresponding author at: University of Rome "Foro Italico", Piazza Lauro de Bosis, 15, 00135 Roma, Italy. Fax: +39 0636733387.
E-mail address: francesco.dirusso@uniroma4.it (F. Di Russo).
URL: http://digilander.libero.it/francesco.di_russo (F. Di Russo).

1053-8119/$ – see front matter © 2012 Elsevier Inc. All rights reserved.
http://dx.doi.org/10.1016/j.neuroimage.2012.11.022

The main purposes of the present study were (1) to find electrophysiological correlates of the motion area V6 using wide-field coherent motion stimuli intentionally designed to best activate the area based on finding in Pitzalis et al. (2010) and (2) to define the temporal relationship between the activity observed in the medial area V6 and that in the lateral area MT+. A third purpose of this study was to determine the spatio-temporal profile of the motion coherency effect on visual evoked potentials (VEPs) and to localize its neural generators. Given the low spatial resolution of VEP data, to improve spatial localization we used the combined VEPs/fMRI technique developed and utilized by our group in previous studies (e.g., Di Russo et al., 2002, 2003, 2005, 2007, 2011; Pitzalis et al., 2012). Cortical sources were identified using dipole modeling based on a realistic head model, taking into account the loci of cortical activation revealed by fMRI in response to the same stimuli. These sources were also localized with respect to classic visual cortical areas (including V6 and MT+) identified in flat maps of individual subjects by wide field retinotopic mapping (e.g., Pitzalis et al., 2006; Sereno et al., 1995) and functional localizers (Pitzalis et al., 2010; Tootell et al., 1995).

Material and methods

Subjects

Twenty-six paid volunteer subjects (mean age of 25.8, range of 19–36 years, 14 females) participated in the main VEP experiment. A subset of 13 of these subjects (mean age 26.4 range of 21–36 years, seven females) also received structural MRI and fMRI scanning. All subjects were right-handed and had normal or corrected-to-normal vision. All participants gave written informed consent prior to both electrophysiological and neuroimaging measures, and all procedures were approved by the ethics and human subjects committees of the Santa Lucia Foundation. Before scanning, subjects were allowed, if they desired, to consume caffeinated beverages to better maintain alertness during the scan session. Each subject participated in up to five scanning sessions.

VEP experiment

Stimuli

Visual stimuli consisted of 3D "star fields" composed by 150 high-contrast random dots (light dots on a dark background) simulating different flow patterns. Global patterns of optic flow were produced by controlling the coherency of local motion directions of the dots. Two kinds of motion were considered: coherent and incoherent motion. For the coherent motion condition a 3D spiral was used consisting in the combination of radial components (all dots moved outwards or inward ($p = 0.5$) at 30°/s along the radii to produce an impression of expansion or contraction) and rotational component of 180°/s (30 rpm) either clock- or counterclockwise ($p = 0.5$). For the incoherent motion condition, the dots randomly moved changing their local direction and speed at random. Average speeds were as in the other coherent motion condition. The purpose was to provide a control condition in which local motion was present in all directions at all locations, with no global flow structure. Both speed and size were logarithmically scaled with eccentricity (i.e., as a function of the distance from the center of the display). The dot diameter varied from 0.1 to 0.5°. In both conditions, each dot traveled along an appropriate trajectory for a limited lifetime of 300 ms, after which it disappeared to be regenerate at a new random position. The appearance of new dots was controlled to maintain constant dot density. A static pattern taken from a single frame of the coherent motion was also used. Stimuli duration was 500 ms showing, in a pseudo-randomized order, one of the three stimuli. Stimulus onset asynchrony varied from 1000 to 2000 ms to avoid motion after-effects. All stimuli were displayed on a 26″ CRT monitor (refresh rate 100 Hz) subtending 80°×60°. Stimuli were presented and synchronized to the electroencephalogram (EEG) using Presentation software (Neurobehavioral Systems, Inc. Albany, CA USA).

Electrophysiological recording and data analysis

The ERP experiment was conducted at the Psychophysiology Laboratory of the University of Rome "Foro Italico" (Rome, Italy). During the EEG recordings, subjects were comfortably seated in a dimly lit, sound-attenuated and electrically shielded room while stimuli were presented in binocular vision on a video monitor. Subjects were trained to maintain stable fixation on a central cross (0.4°) throughout stimuli presentation. The EEG was acquired using a BrainVision™ system (BrainProducts, Germany), with 64 electrodes placed according to the 10–10 system montage. This system and recording technique have already been detailed in previous papers by our group (Di Russo et al., 2005, 2007, 2011; Pitzalis et al., 2012). All scalp channels were referenced to the left mastoid (M1). Horizontal eye movements were monitored with a bipolar recording from electrodes at the left and right outer canthi. Blinks and vertical eye movements were recorded with an electrode below the left eye, which was referenced to site Fp1. The EEG was digitized at 250 Hz with an amplifier band-pass of 0.1 to 100 Hz including a 50 Hz notch filter and was stored for off-line averaging. Computerized artifact rejection was performed prior to signal averaging in order to discard epochs in which deviations in eye position, blinks, or amplifier blocking occurred. On average, 9% of the trials were rejected for violating artifact criteria.

Time locked ERPs to standard stimuli were averaged separately according to the displayed stimulus (coherent motion, incoherent motion, and static pattern). The EEG was segmented into 1100 ms epochs that began 100 ms prior the stimulus onset to establish a voltage baseline. In order to reduce high-frequency noise, the averaged ERPs were low-pass filtered at 35 Hz. Data were re-referenced to averaged mastoids. VEP latency and amplitude components were measured as peak voltage deflections within specified time intervals (see Results section); these measures were taken at the electrode sites where the components were maximal in amplitude.

One-way ANOVAs were used to evaluate the effect of stimulus type (coherent, incoherent and static) on each component, using peak amplitude and latency. The confidence level was set to 0.05 after Greenhouse–Geisser correction.

Modeling of ERP sources

Topographical mapping of scalp voltage and estimation of the dipolar sources of the VEP components in the grand-average waveforms were carried out using Brain Electrical Source Analysis (BESA 2000 v.5.1.8; Megis Software GmbH, Gräfelfing, Germany). The algorithm implemented in BESA estimates the location and orientation of multiple equivalent dipolar sources by calculating the scalp distribution obtained for a given dipole model (forward solution) and comparing it to the actual VEP distribution. Interactive changes in the location and orientation of the dipole sources lead to minimization of the residual variance (RV) between the model and the observed spatio-temporal VEP distribution. In the current study, this analysis used a realistic approximation of the head, with the radius obtained from the average of the group of subjects (81 mm). This realistic head model uses finite elements derived from an average of 24 individual MRIs and consists of three compartments: brain (including the cerebral spinal fluid), skull and scalp. A spatial digitizer recorded the three-dimensional coordinates of each electrode and three fiducial landmarks (the left and right preauricular points and the nasion). A computer algorithm was used to calculate the best-fit sphere that encompassed the array of electrode sites and determine their spherical coordinates. The mean spherical coordinates for each site averaged across all subjects were used for the topographic mapping and source localization procedures. In addition, individual spherical

coordinates were related to the corresponding digitized fiducial landmarks and to landmarks identified on the standard finite element model of BESA 2000. The possibility of interacting dipoles was reduced by selecting solutions with relatively low dipole moments with the aid of an "energy" constraint (weighted 20% in the compound cost function as opposed to 80% for the RV). The optimal set of parameters was found in an iterative manner by searching for a minimum in the compound cost function. In addition to the RV, the quality of the model was evaluated by applying residual orthogonality tests (ROTs; e.g., Bocker et al., 1994).

A mixed (fitting/seeding) strategy was used to model the dipolar sources of the coherent vs. incoherent motion VEPs. Pairs of sources were first fit over specific latency ranges to correspond with the distinctive components in the waveform. These sources were then constrained (seeded) to the closest fMRI activation modulated by the motion coherency and fitted again in orientation only. To minimize cross-talk and interactions between sources, modeling followed a sequential approach according to which dipoles accounting for the earlier portions of the waveform were left in place as additional dipoles were added. Thus, the number of dipoles chosen for these models corresponded to the major topographical features of the differential VEP waveforms.

fMRI experiments

fMRI protocols

In the fMRI experiments, three different experimental designs were used. First, we used an event related fMRI paradigm for the main motion experiment. Second, we used two-condition stimuli and a block sequence paradigm (eight 16 s ON, 16 s OFF epochs) to map the well-known motion area MT+. Third, we used periodic stimuli and a phase-encoded paradigm to map retinotopy of visual cortical areas, and in particular of area V6 together with its borders and extent. The three different fMRI protocols are described below.

Main fMRI experiment: three-dimensional coherent and incoherent motion (3D-CIM)

In the main event-related fMRI experiment, hereafter called 3D-CIM experiment, the motion stimulation and task were identical to those used in the VEP experiment, except for an additional control condition and number and duration of the runs. The additional control condition was represented by null trials, i.e., periods in which only a central cross was displayed on the black background. The null trials constituted a low-level baseline for the study.

Overall, we separately investigated two motion conditions (spiral and random motion) together with two control conditions (static and null trials) for a total of four experimental conditions. Trials were 3 s periods showing one of the four conditions while subjects had to fixate a central red cross of 0.4°. The inter-trial interval was set to zero so that the movies were displayed one after the other to avoid that the brisk switch on-off of the movies could bias the neural response in the regions of interest. The experiment was constituted by 15 trials for each of the four conditions for a total of 60 trials. Except for null trials (presented as a sequence of three consecutive null trials every 18 trials), trials were arranged in a pseudo-randomized order which was different for each scan but fixed across subjects.

MT+ mapping. Two additional scans were acquired to localize the motion-sensitive region, MT+. Stimuli produced by an X11/OpenGL program (original GL code by A. Dale, ported and extended by M. Sereno) consisted of concentric, thin, light gray rings (0.2 cycles/degree, duty cycle = 0.2) on a slightly darker-gray background, either moving (7°/s ON period) or stationary (OFF period). During the ON block, the concentric rings periodically contracted and expanded (1 s, 1 s) to avoid generating motion aftereffects during the OFF block. The average luminance of the stimulus was 61 cd/m^2. The stimulus luminance contrast was low (~1.5%), as described in Tootell et al. (1995), to better isolate MT+. It is now generally acknowledged that the relatively large motion-sensitive region found using this localizer and originally labeled V5 (or MT) in humans (Tootell et al., 1995) is probably a complex of several areas (Kolster et al., 2010; Pitzalis et al., 2010). For this reason, here we referred to it as the "MT complex" or "MT+."

Retinotopic mapping. We mapped the polar angle (measured from the contralateral horizontal meridian around the center of gaze) and eccentricity (distance from the center of gaze) using the same phase-encoded retinotopic stimuli previously used to map the visuotopic organization of human area V6 (Pitzalis et al., 2006; Sereno et al., 1995). High contrast light and dark colored checks counterphase flickered in either a ray- or a ring-shaped configuration (polar angle and eccentricity, respectively). The average luminance of the stimuli was 105 cd/m^2. Each subject was presented with periodic stimuli (64 s/cycle, 8 cycles/scan), varying in eccentricity or polar angle, in at least two pairs of scans. Stimuli moved slowly and continuously, and checks reversed between bright and dark at a rate of 8 Hz. The retinotopic mapping allowed us to map visual cortical areas, including V6, and to recognize which ones were activated by the stimuli we used.

Apparatus and procedures

The MR examinations were conducted at the Santa Lucia Foundation (Rome, Italy) on a 3T Siemens Allegra MR system (Siemens Medical Systems, Erlangen, Germany) equipped for echo-planar imaging. Single-shot echo-planar imaging (EPI) images were collected using blood-oxygenation-level-dependent imaging (Kwong et al., 1992) by a standard transmit-receive birdcage head coil.

Stimuli were generated by control computers (a standard PC and an SGI O2, both equipped with a standard 3D graphics card) located outside the MR room and running different software for each specific experiment. For the 3D-CIM experiment, stimuli were presented with an in-house software, implemented in MATLAB (The MathWorks Inc., Natick, MA, USA) using Cogent 2000 (developed at FIL and ICN, UCL, London, UK) and Cogent Graphics (developed by John Romaya at the LON, Wellcome Department of Imaging Neuroscience, UCL, London, UK). For the MT+ localizer scan and the retinotopic mapping, stimuli were presented with an in-house OpenGL program (Mapper software) code by A. Dale and M. Sereno.

Visual stimuli were projected using an LCD video projector with a customized lens to a back projection screen mounted behind the MR tube and visible through a mirror placed inside the head coil. For all experiments a wide-field screen was used, and the standard mirror was enlarged so that the most peripheral part of the screen was in view. This setup allowed a field of view that subtended 69° horizontally, 55° vertically, and 82° in an oblique direction. Besides better revealing cortical areas that represent the periphery, such wide field retinotopic stimulation also helped to avoid confounds in fMRI mapping due to surround inhibition. As explained previously (e.g. Pitzalis et al., 2006), retinotopic cortical regions having representations of visual space just beyond the peripheral edge of a rotating wedge can generate a periodic signal with a misleading 180° phase offset. By stimulating most of the visual field, such phase inversion is greatly reduced. In all experiments, fixation distance and head alignment were held constant by a chin rest mounted inside the head coil. Subjects' heads were stabilized with foam padding in order to minimize movement during the scans. All experiments used passive viewing and subjects were required to gaze at a central cross throughout the period of scan acquisition.

Imaging parameters

The 30 coronal slices were 2.5 mm thick (with a 0 mm gap, interleaved excitation order), with an in-plane resolution of 3 × 3 mm, oriented approximately perpendicular to the calcarine fissure. This voxel

size strikes a compromise between sufficient signal-to-noise and the ability to assign activations to the correct sides of the sulci and gyri.

Each participant underwent six scans for the 3D-CIM experiment, four scans for the localizer and six scans for the retinotopic mapping (three runs for each stimulus type-eccentricity and polar angle). Each scan took either 180 s (3D-CIM), 256 s (localizer scans) or 512 s (retinotopy), with 92, 128 or 256 single-shot EPI images per slice, respectively (TR = 2 s, TE = 30 ms, TA = 66.6 ms, flip angle = 70°, 64×64 matrix, bandwidth = 2298 Hz/pixel). In each scan, the first 8 s of the acquisition were discarded from data analysis in order to achieve a steady state, and the experimental tasks started at the beginning of the fifth volume. Overall, a total of 208 scans were carried out on the 13 subjects (78 scans for the 3D-CIM experiment, 52 scans for the functional localizer and 78 scans to map retinotopic visual areas).

The cortical surface of each subject was reconstructed from a pair of structural scans (T1-weighted MPRAGE, 176 contiguous sagittal slices, 1×1×1 mm; TR = 2000 ms, TE = 4.38 ms, flip angle = 8°, matrix 256×256, bandwidth = 130 Hz/pixel) taken in a separate session. The last scan of each functional session was an alignment scan (also MPRAGE, 1×1×1 mm) acquired in the plane of the functional scans. The alignment scan was used to establish an initial registration of the functional data with the surface. Additional affine transformations that included a small amount of shear were then applied to the functional scans for each subject using blink comparison with the structural images to achieve an exact overlay of the functional data onto each cortical surface.

Data analysis

Anatomical image processing

FreeSurfer was used for surface reconstruction (Dale et al., 1999; Fischl et al., 1999). High resolution structural images obtained from each subject were manually registered and averaged. After reconstructing each hemisphere, we completely flattened the inflated occipital lobe after first cutting it off posterior to the Sylvian fissure, and making an additional cut along the Calcarine fissure. Stereotaxic coordinates were calculated through an automatic nonlinear stereotaxic normalization procedure (Friston et al., 1995), performed using the SPM8 software platform (Wellcome Department of Cognitive Neurology, London, UK), implemented in MATLAB (The MathWorks Inc., Natick, MA, USA).

Functional image processing: main experiment and localizer scans

Images from the main experiment and functional localizer were preprocessed and analyzed using SPM8 (Wellcome Department of Cognitive Neurology, London, UK). Functional time series from each subject were first temporally corrected for slice timing, using the middle slice acquired in time as a reference, and then spatially corrected for head movement, using a least-squares approach and six-parameter rigid body spatial transformations. They were then spatially normalized using an automatic nonlinear stereotaxic normalization procedure (final voxel size: 3×3×3 mm) and spatially smoothed with a three-dimensional Gaussian filter (6 mm full-width-half-maximum). The template image for spatial normalization was based on average data provided by the Montreal Neurological Institute (Mazziotta et al., 1995) and conforms to a standard coordinate referencing system (Talairach and Tournoux, 1988). The time series of functional MR images was first analyzed separately for each participant. The effects of the experimental paradigm were estimated on a voxel-by-voxel basis, according to the general linear model. For MT+ localizer scans, stimulation blocks were modelled as box-car functions spanning the whole block duration and convolved with a standard hemodynamic response function. Significance was judged at the voxel level and by cluster size. For the 3D-CIM experiment, the onset of each trial constituted a neural event, which was modeled through a canonical hemodynamic response function, chosen to represent the relationship between neuronal activation and blood flow changes. Separate regressors were included for each trial type (spiral, random, static and fixation), yielding parameter estimates for the average hemodynamic response evoked by each trial type. The model also included a temporal high-pass filter, to remove low-frequency confounds with a period above 128 s. Serial correlations in the fMRI time series were estimated with a restricted maximum likelihood (ReML) algorithm using an autoregressive AR(1) model during parameter estimation, assuming the same correlation structure for each voxel, within each run. The ReML estimates were then used to whiten the data. These subject-specific models were used to compute a set of contrast images per subject, each representing the estimated amplitude of the hemodynamic response in one trial type relative to the fixation baseline. Contrast images from all subjects were entered into a within-subjects ANOVA with non-sphericity correction, where subject was considered as a random effect, thus allowing to draw inferences related to the whole population our participants were extracted from.

We used the same model used in the ERP data analysis to search for brain regions differentiating coherent from the incoherent motion. We performed two main contrasts: coherent (spiral) vs. incoherent (random) motion (contrast C–I) and incoherent (random) vs. coherent (spiral) motion (contrast I–C). The resulting statistical parametric map of the F statistics was thresholded at the voxel level and by cluster size. Correction for multiple comparisons was performed using false discovery rate ($p<0.05$; extent threshold = 10 voxels). Regions were defined as clusters of significantly activated adjacent voxels at most 8 mm away from each local maximum of the statistical map. The resulting regions include all voxels showing a reliable BOLD response greater for the coherent (contrast C–I) or incoherent (contrast I–C) motion. For each subject and region, we computed an estimate of the averaged amplitude of the hemodynamic response in each experimental condition (spiral, random and static), by entering a spatial average (across all voxels in the region) of the pre-processed time series into the individual general linear models. Such regional hemodynamic response estimates were then analyzed through a repeated-measures analysis of variance ($p<0.05$). The *post-hoc* Duncan's test was performed when appropriate ($p<0.05$). In-house software (BrainShow, written in Matlab) was used to visualize the resulting regions onto a population-average, landmark- and surface-based (PALS) atlas (Van Essen, 2005), and to assign anatomical labels to activated areas at the level of Brodmann areas and cortical gyri. Brodmann areas were derived from the Talairach Daemon public database (Lancaster et al., 2000), while cortical gyri were derived from a macroscopical anatomical parcellation of the MNI single-subject brain (Tzourio-Mazoyer et al., 2002). BrainShow (code by G. Galati) has been used in previous studies from our and other groups (e.g. Castriota-Scanderbeg et al., 2005; Galati et al., 2008, 2011; Ionta et al., 2011; Pitzalis et al., 2010) and is freely available on request for academic usage.

Analysis of retinotopic data

Retinotopic data were analyzed using FreeSurfer (Dale et al., 1999; Fischl et al., 1999) by means of a Fourier transform (FT) of the MR time course from each voxel after removing constant and linear terms. This generated a vector with real and imaginary components for each frequency that defined an amplitude and phase of the periodic signal at that frequency. To estimate the significance of the correlation between the blood oxygenation level-dependent (BOLD) signal and the stimulus frequency (8 cycles per scan), the squared amplitude of the signal at the stimulus frequency was divided by the mean of squared amplitudes at all other "noise" frequencies (excluding low-frequency signals due to residual head motion and harmonics of the stimulus frequency). This ratio of two chi-squared statistics follows the F-distribution with degrees of freedom equal to the number of time points and can be used to calculate a significance P-value. These analysis methods were similar to those used in many previous studies (e.g.,

Hagler and Sereno, 2006; Pitzalis et al., 2006, 2010; Sereno et al., 1995; Tootell et al., 1997). The boundaries of retinotopic cortical areas (V1, V2, V3, VP, V3A, V6, V7, V4v and V4/V8) were defined on the cortical surface for each individual subject on the basis of phase-encoded retinotopy (e.g. Sereno et al., 1995) and subsequent calculation of visual field sign. This method provides an objective means of drawing borders between areas based on the angle between the gradients (directions of fastest rate of change) in the polar angle and eccentricity with respect to cortical position (Sereno et al., 1995).

Results

Electrophysiological results

The VEP waveforms elicited at relevant electrode sites by stimuli in each of the three stimulation conditions (coherent motion, incoherent motion, static pattern) are shown in Fig. 1, and topographical features of the major components in the scalp distribution maps are shown in Fig. 2.

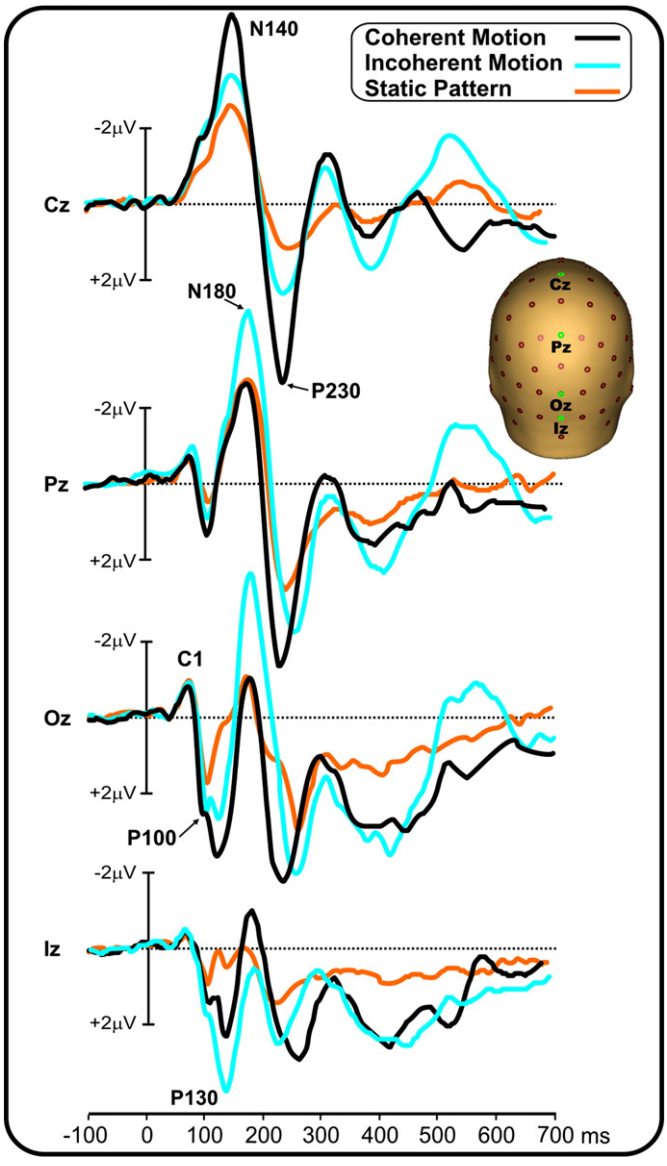

Fig. 1. Grand averaged waveforms of the VEPs in each of the three conditions for relevant sensor whose locations are indicated on the head representation. Main components are labeled.

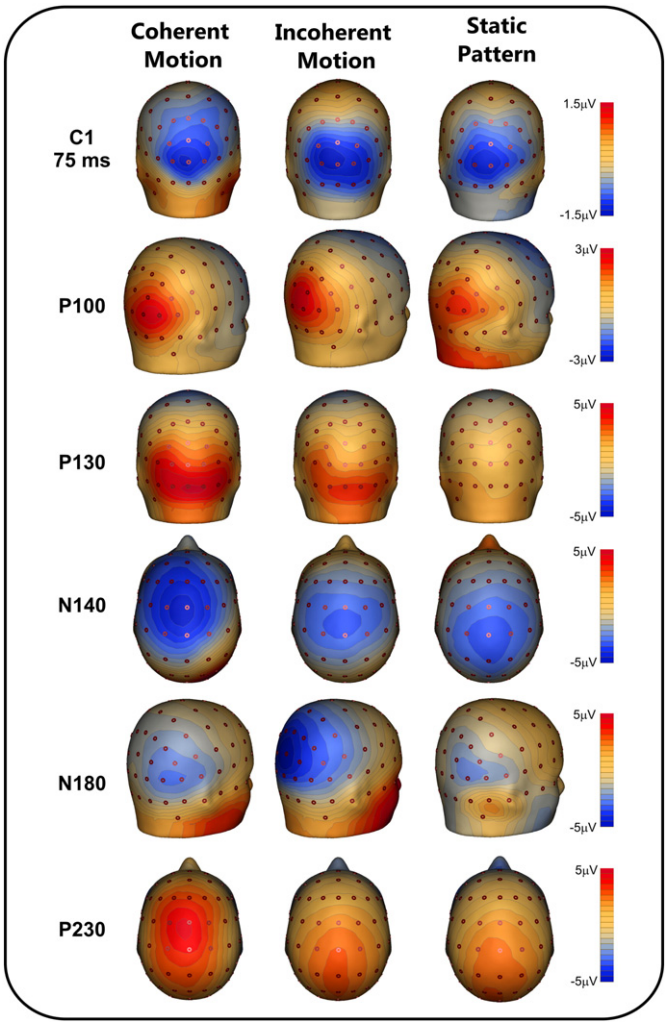

Fig. 2. Spline-interpolated 3D voltage maps of the VEP components found in the grand averaged waveforms in the three conditions.

The earliest component (labeled C1) had an onset of approximately 50 ms and a peak latency of 75 ms. The C1 component was negative and most prominent at medial occipital sites. No significant amplitude difference was found between conditions. Following the C1, a positive deflection (P100) was elicited over bilateral occipital sites with a peak latency of 100 ms. Even though the P100 was slightly larger for the two motion stimuli ($p = 0.08$), no significant amplitude difference were found between conditions. With a peak latency of 130 ms, a further positive component (P130) focused on ventral occipito-temporal sites. The P130 for the motion conditions were larger ($p<0.01$) than for the static pattern, where it resulted nearly absent. Furthermore, the P130 for coherent motion was larger ($p<0.05$) than for incoherent motion.

In the N2 interval between 140 and 200 ms, two temporally overlapping negative waves were elicited concurrently; an initial anterior peak (N140) was prominent on medial central sites. The N140 topography was more anterior for the coherent motion, more posterior for the static pattern and an half-way distribution for the incoherent motion condition. The N140 was larger for the coherent motion ($p<0.01$) than for the other two conditions, which did not differ. A second negative deflection (N180) was prominent at lateral parieto-occipital sites, and was more medial for the incoherent motion conditions. The N180 for the incoherent motion was larger ($p<0.01$) than for the other two conditions, which did not differ.

In the P2 interval between 200 and 300 ms, a large positivity (P230) dominated the waveforms. This component peaked on medial

central sites with a radial distribution similar to the N140 (but opposed in polarity) also more anterior for the coherent motion condition. The P230 for the coherent motion was larger ($p<0.01$) than for the other two conditions. Furthermore, the P230 for the incoherent motion was larger ($p<0.05$) than for the static pattern.

In none of these components, significant latency differences were found between conditions. However the P230 peak latency was earlier ($p=0.07$) for the coherent (230 ms) than for incoherent motion (255 ms).

Fig. 3A shows an overview of the aforementioned statistical comparisons and is worth of note that the motion coherency specifically modulated the activity over 100 ms after the stimulus onset, enhancing the P130, the N140 and the P230, but reducing the N180 component. To extract from VEP signals the activity specifically related to the motion coherency, difference waves were obtained subtracting the incoherent from the coherent motion condition (Fig. 3B). Scalp topography showed that the larger P130 of the coherent motion was focused on bilateral temporo-occipital ventral cortex. The larger activity of the N140 and the P230 for the coherent motion showed similar distribution peaking on medial central sites. The larger N180 for the incoherent motion focused on medial parieto-occipital sites.

Imaging results

We selected regions showing an fMRI response greater for either the coherent (contrast C–I) or the incoherent (contrast I–C) motion (see Material and methods section for details). Results from these contrasts revealed significant bilateral activations in three cortical regions, which are displayed together on the semi-inflated cortical surface reconstruction of both hemispheres of the average brain (Fig. 4A). Mean percentage signal changes (averaged between the hemispheres) in the motion conditions and in the static frames relative to the baseline (i.e., fixation) are plotted in Fig. 4A (see histograms on the left).

One motion region was located in the medial parieto-occipital sulcus (POs) (Fig. 4A, green region). Its location corresponds well to the definition of human area V6 provided by our group (Pitzalis et al., 2006, 2010). The area indeed is located on the dorsal margin of the POs and has the following Talairach coordinates ($x=\pm11$, $y=-78$, $z=+35$; Table 1), very similar to the coordinates of area V6 that we reported in our original paper (Pitzalis et al., 2006) ($x=\pm9$, $y=-78$, $z=+37$). The medial POs motion region responds more to any type of motion than to static stimuli and much more to coherent than to incoherent stimuli (72% of signal change).

Another motion region was located bilaterally in the temporal cortex (Fig. 4A, red region). The mean Talairach coordinates of this region ($x=\pm44$, $y=-66$, $z=5$; Table 1) are in good agreement with those of the classic motion sensitive region MT+ described in earlier studies using both PET ($x=\pm42$, $y=-67$, $z=0$; Watson et al., 1993) and fMRI ($x=\pm45$, $y=-72$, and $z=3$; Tootell et al., 1995). The middle temporal motion region responds more to any type of motion than to static stimuli and more to coherent than to incoherent stimuli (20% of signal change).

Finally, a third motion region was located in the posterior segment of the intraparietal sulcus (pIPs, Fig. 4A, blue region). The mean coordinates of this region are $x=\pm24$ $y=-85$ $z=25$ (Table 1). They fit well with the coordinates given by Tootell et al. (1997) for the superior medial end of their V3A area ($x=\pm14$; $y=-84$; $z=+19$) which corresponds to the peripheral field representation in V3A. The activation on the pIPs does not extend either medially or antero-laterally toward the typical positions of retinotopic dorsal areas V3 and V7, respectively. The activation is dorsally located and is distinct from POs ROI, being immediately posterior and lateral to it and bordering its posterior part. The motion region near the pIPs responds more to any type of motion than to static stimuli and more to incoherent than to coherent stimuli (25% of signal change).

VEP–fMRI combination

Combination of VEP and fMRI data allowed to determine the timing of the neural response modulated by motion coherency. Initially, the VEP data alone were used to create a raw multi-source model using the BESA algorithm (unseeded model, white circles in Fig. 4A). This source model was calculated for the coherent minus incoherent difference wave. Based on the imaging results showing bilateral activity, three symmetrical pair of sources were used. A first source pair was optimized to fit the N130 activity in the 120–140 ms time windows, obtaining a localization in ventro-lateral occipito-temporal areas. A second pair fitting the N140 (130–150) was localized in the superior parietal lobule (SPL), not far from the dorso-medial parieto-occipital areas. A third pair fitting the N180 (170–190) was localized in extrastriate occipital areas of the dorsal stream. A fourth pair fitting the P230 (200–250) was also localized again in the SPL near the dorso-medial

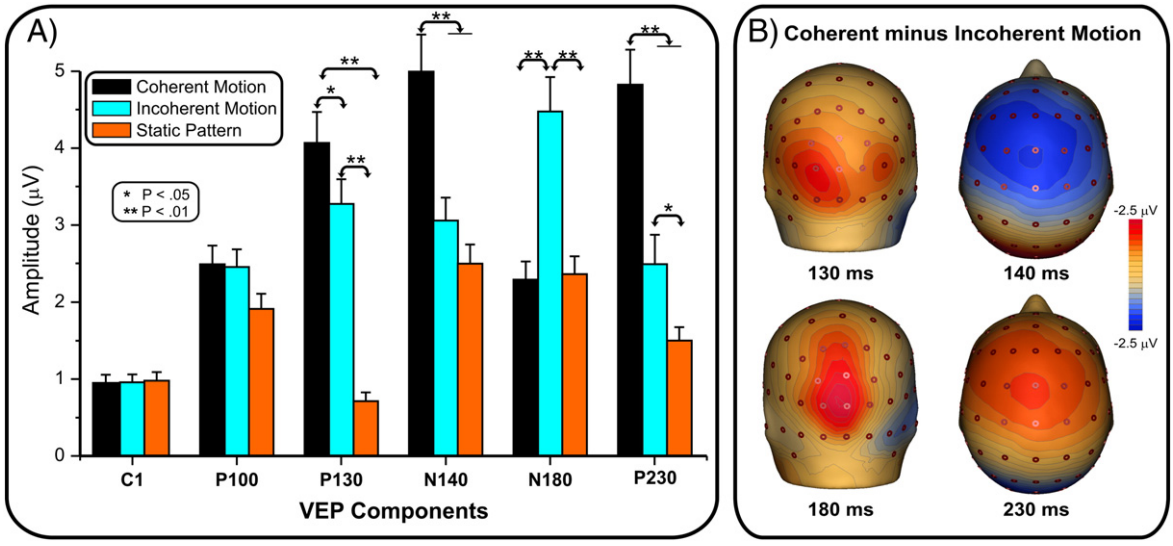

Fig. 3. A) Peak amplitudes of the found VEP components in the three conditions. Statistical significant differences are marked by stars. B) Spline-interpolated 3D voltage maps of the significant activity found in the coherent minus incoherent difference wave.

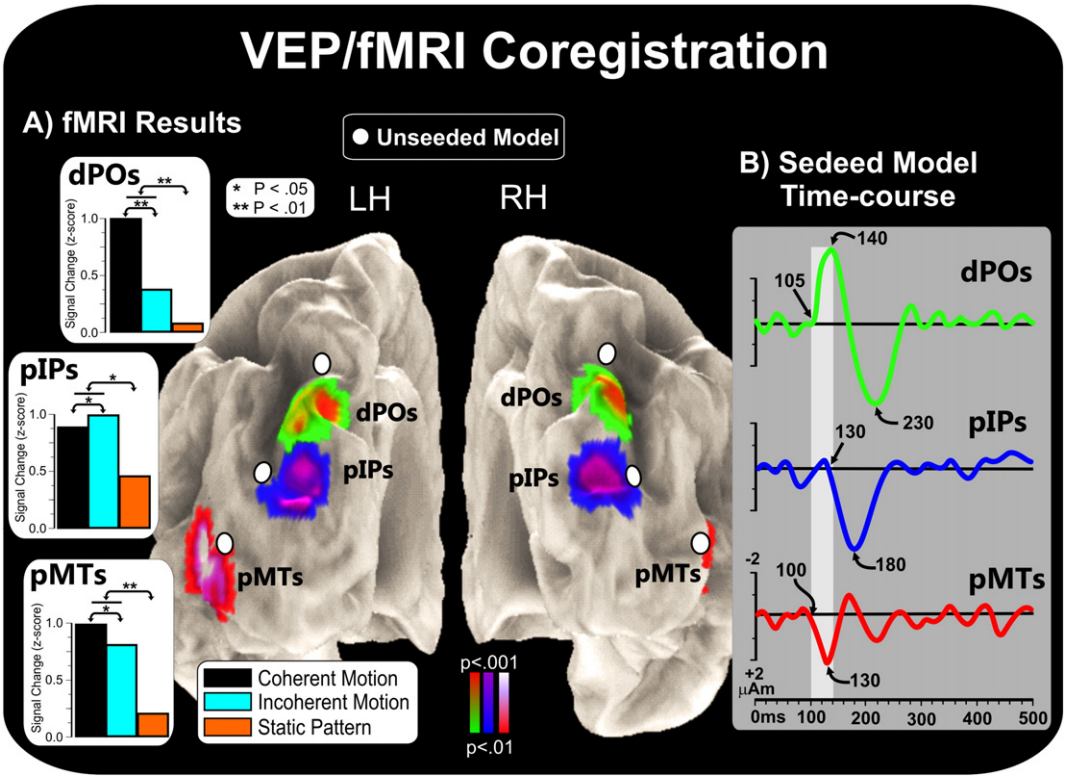

Fig. 4. (A) Group-averaged Imaging results. Regions more activated in the coherent or incoherent motion conditions (contrasts C–I and I–C) are indicated on the cortical surface using the sulcal anatomy labels: dPOs (dorsal Parieto-Occipital sulcus), pIPs (posterior end of the Intraparietal Sulcus) and pMTs (posterior Middle Temporal sulcus). Results are displayed together on the semi-inflated cortical surface reconstruction of the left and right hemispheres of the average brain. Histograms on the left represent the averaged BOLD percent signal change obtained in the three areas across subjects and hemispheres for the two motion (Coherent and Incoherent) and static conditions. (B) Source waveforms of the dipoles fit to the grand averaged VEPs and seeded to the fMRI activations (listed in Table 1). White circles show the source locations in the unseeded dipole model of the coherent minus incoherent difference wave. The light gray area indicates the 100–140 ms time window. (For interpretation of the references to color in this figure legend, the reader is referred to the web version of this article.)

parieto-occipital areas almost overlapping to the N140 sources. These sources reduced the RV less than 0.3% indicating that the P230 component was already well explained by the N140 source and for this reason was not included in the model. All the remaining three sources pairs were then optimized in the time range of 120–250 ms and this model explained most of the activity, leaving a RV of 2.7%.

Following the analysis previously described by our group (e.g., Di Russo et al., 2011), regions of interest were then selected by clustering the fMRI spots for the same contrast (coherent vs. incoherent stimuli). The resulting coordinates of these regions (see Table 1) were compared to the locations of unseeded model to create a final model based on the closest fMRI spot, with the source orientations optimized to the new locations (seeded model). The rationale for this strategy was to use the fMRI information to solve the inverse problem of the source localization. Fig. 4B shows the source time course (dipole moment) in the fMRI seeded locations (centre of the fMRI foci in Fig. 4A) averaged between the hemispheres. The N130 source resulted closest to the fMRI spot in the pMTs. This source (red wave) began its activity at 100 ms and peaked at 130 ms; then showed a small negative peak at 170 ms. The N140 source resulted closest to the medial dPOs activation. The time course of this source (green wave) accounted for the N140 modulation beginning at 105 ms and peaking at 140 ms; this source also well accounted for the P230 component showing a second large peak at 230 ms. In other words the source in the dPOs showed two peak activities one earlier at 140 and a second at 230 ms. Note that in the 100–140 ms, only pMTs and dPOs sources were active (light gray area in Fig. 4B) windows. The N180 source was closest to the pIPS activations with an onset at 130 ms and peak at 180 ms (blue wave). This multi-source model accounted for the 97.0% of the variance of the scalp voltage topography over the 120–250 ms time range. These findings, demonstrating that the seeded model only accounted for slightly more variance than the unseeded model (3.0% versus 2.7%), suggest that the seeded model well accounted for the sources of the motion VEPs that corresponded to the sites of the fMRI activations.

Given that the N140 and P230 components were localized in the dorsal SPL where other parietal areas are located, we performed additional analysis on the VEP data to rule out alternative parietal origin of the two components. We considered the possibility that the source of the N140 and P230 components could be the ventral intraparietal (VIP) area which is more anterior and lateral than dPOs. Although we did not observe VIP activity in the average fMRI map, in previous studies this area has been found to respond well to coherent optic flow and less well to random motion (e.g., Bremmer et al., 2001; Cardin and Smith, 2010, 2011; Sereno and Huang, 2006; Smith et al., 2012; Wall and Smith, 2008). Thus, instead of seeding the N140/P230 source in the dPOs, we seeded them in the VIP area using the coordinates published by Bremmer et al., 2001 (Talairach coordinates −40, −40, 42 and 38, −44, 45). Results showed that the residual variance of the model

Table 1
Mean Talairach coordinates of ROIs identified in the present study comparing the coherent and incoherent motion conditions in the averaged fMRI data from thirteen subjects. The table shows the coordinates of the maxima of the motion activated regions (values are in mm). All maxima were significant at $p<0.05$ (whole brain, Bonferroni corrected).

	Talairach coordinates		
ROIs	X	Y	Z
dPOs (V6)	±11	−78	35
pMTs (MT+)	±44	−66	5
pIPs (V3A)	±24	−85	25

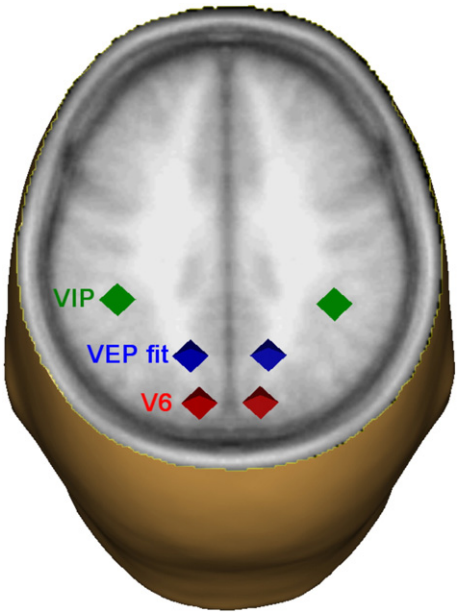

Fig. 5. Brain template (transversal plane) with superimposed the location of VIP area (green spots), of the N140/P230 component fit (blue spots), and of the V6 area. The VEP based localization of the N140/P230 was much closer to V6 than VIP. (For interpretation of the references to color in this figure legend, the reader is referred to the web version of this article.)

seeded in the dPOs was 3.0%, while increased to 6.8% if seeded in the VIP area, reinforcing the idea that the dPOs is the most probable source of the N140 and P230. We also plotted the location of the VIP, V6 and the VEP fit of the N140/P230 on the same brain template. As evident by Fig. 5 the VEP based localization of the N140/P230 was much closer to V6 than VIP.

Other visually responsive areas besides VIP exist along the length of the IPS. These have been called DIPSA, DIPSM and POIPS according to a functional classification scheme (Orban et al., 2003; Sunaert et al., 1999) and IPS1/2/3 according to a retinotopic scheme (Silver et al., 2005; Swisher et al., 2007). Some of these areas lie closer to the N140 VEP source than either VIP or V6, raising the possibility that one or more of these areas may give rise to the source of N140. These areas are sensitive to motion and to structure-from-motion. However, there are no reports in the literature of a preference for coherent over incoherent optic flow and they are not active in our C-I contrast. We therefore think it is unlikely that they give rise to N140, but this cannot be ruled out, in view of their close proximity to the identified VEP source. Another possibility might be that N140 arises mainly from V6 but that there is some contribution from IPS areas, leading to an apparent source near V6 but shifted towards the IPS.

Single subject fMRI activations

Retinotopic mapping was performed to demarcate striate and extrastriate visual areas, so as to illustrate the exact relationship between the motion-related fMRI activations and the known early visual cortical areas. Retinotopic dorsal (V1, V2, V3, V3A, V6, V7) and ventral (V1, V2, VP, V4v, V4/V8) visual areas were successfully identified by mapping quadrant representations and visual field signs (see Material and methods section). In addition, the classic lateral motion area MT+ was individually mapped by functional localizer (Tootell et al., 1995). The boundaries of all these visual areas were rendered on a flattened version of each participant's reference anatomy. Activations in striate and adjacent extrastriate visual areas could be distinguished despite their close proximity and individual differences in cortical anatomy. In Fig. 6 the motion-related fMRI activations (C–I contrast, red; I–C contrast, blue) are displayed together on the flattened representation of the left and right hemisphere of a representative participant. On the flat map, fMRI results have been overlaid with a set of lines representing the boundaries of early visual areas that we defined in this subject.

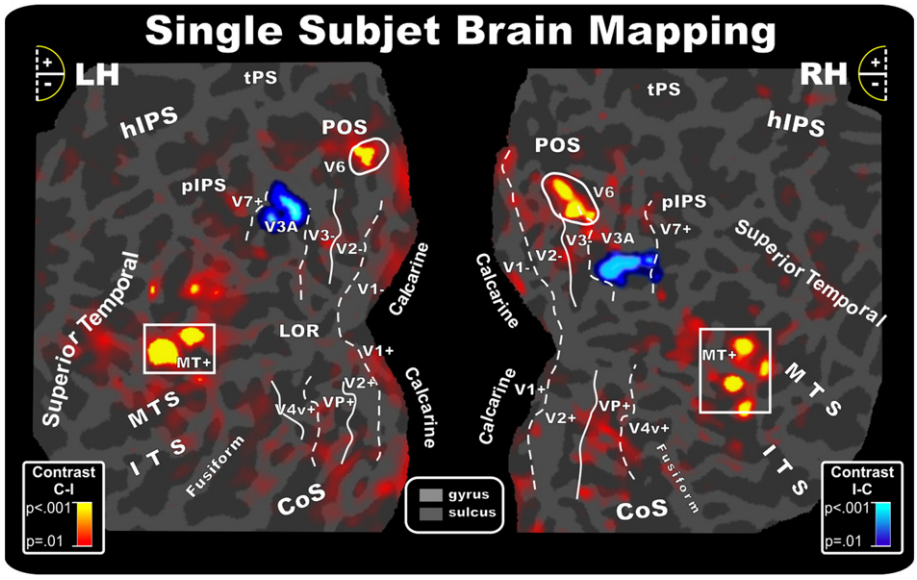

Fig. 6. Motion-related fMRI activations projected onto the flattened left and right hemispheres of an representative participant. Regions more activated in the coherent (red) or incoherent (blue) motion conditions (contrasts C–I and I–C) are shown in relation to the boundaries of visual areas defined in the same subject by the retinotopic visual field sign. The box surrounding MT+ represents the location of the motion sensitive region defined in this subject based on separate localizer scans. As indicated in the semicircular logos, dashed and solid lines correspond to vertical and horizontal meridians, respectively; the plus and minus symbols refer to upper and lower visual fields representations, respectively. The pseudocolor scale in the left of the figure indicates the statistical significance of the fMRI activations. Major sulci (dark gray) are labeled as follows: parieto-occipital sulcus (POS), transverse segment of the parietal sulcus (tPS), posterior segment of the intraparietal sulcus (pIPS), superior temporal sulcus (Superior Temporal), middle temporal sulcus (MTS), inferior temporal sulcus (ITS), collateral sulcus (CoS), fusiform gyrus (Fusiform), lateral occipital region (LOR), and Calcarine fissure (Calcarine). (For interpretation of the references to color in this figure legend, the reader is referred to the web version of this article.)

In individual data, motion related stimulation activated three typical motion areas in accordance with the group fMRI data. As shown in Fig. 6 for a typical subject, the contrast C–I revealed significant bilateral activations in areas V6 and MT+ while the contrast I–C revealed significant bilateral activations in area V3A. This pattern of activations was consistently observed in the majority of subjects: V6 (95%), MT+ (90%), and V3A+ (89%).

The temporal activation occupies an anatomical position in between the Inferior Temporal sulcus (ITs) and the Middle Temporal Sulcus (MTs) and overlaps with the location of the motion-sensitive cortex (MT+; see white boxes) functionally mapped in this subject by additional scans as described in the Material and methods section. The anatomical position of MT+ is in line with the description of this region provided in previous fMRI studies where the same functional localizer has been used (e.g., Tootell et al., 1995).

Based on single-subject mappings like those shown in Fig. 6, the group-averaged fMRI activations produced by motion stimulation may be assigned to specific visual areas. Thus, the activations in the medial POs region (proposed source of the N140 and P230 components) appear to originate primarily from area V6. The mid-temporal activations may be assigned to the motion-sensitive area MT+ (proposed source of the P130). Finally, the mid-occipital activations within the pIPS in the group data correspond to activity in dorsal area V3A (proposed source of the N180).

Discussion

High-resolution EEG recordings combined with neuroimaging data, retinotopic mapping and wide field coherent motion stimulation were here used to follow the flow of motion signals from the occipital pole to the medial and lateral motion areas V6 (Pitzalis et al., 2006, 2010) and MT+ (e.g., Tootell et al., 1995). The increased resolution of combined EEG/fMRI methods enabled us to localize the VEP data within each visual area (e.g. Di Russo et al., 2011) contributing to determine the spatio-temporal profile of the motion coherency effect on VEPs.

We found a complex sequence of six components located in occipital, parietal and temporal cortices, including feed-forward and reentrant feedback signals in some specific cortical regions. Specifically, the processing of motion in the cortical network started in V1 (C1 component) approximately 50 ms after stimulus onset (peaking at 75 ms), then was detected in ventral extrastriate areas, likely LOR region (P100) and, almost simultaneously, in MT+ (P130) and V6 (N140). Subsequently, the activity in the posterior part of the brain was found in V3A (N180) and again in V6 (P230).

Response timing of human motion area V6

Our key finding concerns the response timing of human visual area V6, the less studied among the cortical motion areas. The main result found here is the presence of two VEP components likely arising from V6 in two different temporal windows: first around 100–140 ms (N140 component), and then again, even more strongly, about 100 ms later (P230 component). In other words, after the first early activation V6 was robustly re-activated between 200 and 250 ms in the range of the P2 component.

The early timing of V6 activation (onset latency 105 ms) together with the small temporal gap with the V1 timing (peak latency 75 ms) found here is in agreement with data on macaque brain, where it has been proved the existence of a direct connection between V1 and V6 (Galletti et al., 2001). This result fits also with previous human MEG studies which found visual activity in POS and V1 in a similar latency range—between 60 and 100 ms from stimulus onset (Vanni et al., 2001; von Pföstl et al., 2009).

The late activity of area V6 found here is consistent with that observed in two recent studies by our group where we found a combined VEPs/fMRI activity in area V6 (as defined by its functional localizer as described in Pitzalis et al., 2010) modulated by spatial attention (Di Russo et al., 2011) and fast speed motion stimuli (Pitzalis et al., 2012). In both studies the activity peaked quite late, approximately 200–250 ms after stimulus presentation.

A late parietal activity (detected up to the central electrodes) in the latency range of the P2 was also found in other previous studies (Hoffmann and Bach, 2002; Kremlácek et al., 2004), even though it had never been localized in area V6 which was not even discovered at that time. This late activity was attributed to processing of complex features of motion (expanding/contracting radial motion) and was thought to represent a higher order level of visual processing of biologically important stimuli (e.g. Kuba et al., 2007 for review). Here we show that the analysis of such complex motion signals also occurs much earlier, about 100 ms before (N140), supporting the hypothesis of a V6 involvement in early cortical motion processing. We are aware that EEG cannot reveal connections between cortical regions. However, we speculate that the late activity in V6 (P230) could be a re-entrant feedback from other extrastriate visual areas, like V3A which is strongly connected with V6 in the macaque (Galletti et al., 2001) and is supposed to be involved in extracting form from motion (Vanduffel et al., 2002; Zeki, 1978) and in recognizing the motion of objects in the visual field (Galletti and Fattori, 2003). Again, we speculate that such a type of signal could help V6 to recognize real motion of objects among the plethora of retinal image movements self-evoked by eye and body movements (Galletti and Fattori, 2003; Galletti et al., 1990).

VEP neural generators of the motion coherency effect

The present study provides important results for what concerns the spatio-temporal profile of the motion coherency effect on visual evoked potentials and the localization of its neural generators. As said above, we found a sequence of six different components, but not all these components were affected by the motion coherence. The earliest VEP components, the C1 and P100, were not modulated by motion coherence. Since the original observation of Jeffreys and Axford (1972), the C1 is known to arise from the primary visual area V1. Its localization has been confirmed in many fMRI–VEP studies from our (e.g. Di Russo et al., 2011) as well as other (e.g. Clark et al., 1995; Zhang et al., 2012) laboratories. Reviewing the extensive VEP literature on this component, it is evident that the C1 has been found in response to many visual stimulation paradigms, such as pattern-onset, pattern-reversal and motion-onset (Di Russo et al., 2002, 2005). Therefore, the C1 seems to be a general phenomenon related to the activity of area V1, likely reflecting the cortical volley from the lateral geniculate nucleus. In previous studies (e.g. Pitts et al., 2010; Pitzalis et al., 2012) the P100 has been localized in multiple extrastriate visual areas as V4 and lateral occipital regions (LOR), i.e., the cortex between dorsal areas V3 and MT+ (Larsson and Heeger, 2006; Smith et al., 1998; Tootell and Hadjikhani, 2001). Present results indicate that these early visual areas did not detect motion coherence, even though the P100 in motion conditions was slightly larger than that obtained with static pattern, likely for the contribution from the LOR region which was found to be a motion sensitive region in both electrophysiological (e.g., Pitzalis et al., 2012) and imaging (e.g., Pitzalis et al., 2010; Van Oostende et al., 1997) studies.

Activities in MT+, V6 and V3A were consistently and differently modulated by motion and its coherence. The most robustly modulated visual area is V6. We found that the perception of coherent motion produces in the brain specific VEP components most likely arising from area V6 in two different temporal windows (N140 and P230, see above). Thus, we confirm that human area V6 codes the motion coherence, which evokes in this area a much stronger response than random motion (note in this respect the small V6 response to static and random condition in Fig. 4A). The V6 preference for motion coherency we found here is also in line with recent fMRI human studies which have reported that V6 encodes optic flow, likely for monitoring

and controlling egomotion (e.g., Cardin and Smith, 2010, 2011; Helfrich et al., in press; Pitzalis et al., 2010). We tested the hypothesis that the N140 and P230 components could derive from the VIP area instead of area V6, but the additional analysis performed on the VEP data unable us to rule out alternative parietal origin of these two components (see Results section). Although the lack of activity of area VIP could sound somewhat unexpected, we want to point out that the activity in the VIP area was not consistently found also in some other paper using coherent vs random motion (Fischer et al., 2012; Pitzalis et al., 2010; Sereno et al., 2001). It is possible that VIP responds well to coherent optic flow and less to other type of coherent motion or to single optic flow component as that used in the present study (i.e., spiral).

The coherent motion enhances the activity also in MT+, but only at early latency (P130) and much less strongly than in V6. In human, MT+ is one of the most celebrated motion areas of the dorsal stream (Tootell et al., 1995; Watson et al., 1993; Zeki et al., 1991). Although most of the previous neuroimaging studies support the hypothesis that MT+ does not code motion coherence in that it responds equally to coherent and incoherent motion (e.g., Helfrich et al., in press; Konen and Kastner, 2008; Pitzalis et al., 2010; Previc et al., 2000; Wall and Smith, 2008) there are some studies showing that MT+ is selective to a particular coherent motion stimulus, the optic flow pattern (e.g., Morrone et al., 2000; Wall et al., 2008). Likely, the P130 component found here arises from the neighboring MST area, which is thought to be sensitive to the motion coherence in both macaque (e.g., Duffy and Wurtz, 1991a, b, 1995; Saito et al., 1986) and human (e.g., Kovács et al., 2008; Wall et al., 2008) brain, and which belongs to the so-called MT complex (e.g., Huk et al., 2002). However, the full independent characterization of V5/MT and MST necessary to confirm this claim was not carried out in this work, and the hypothesis that the P130 actually derives from MST remains speculative. This is the reason why we refer to this activation as to MT+ area.

While both areas V6 and MT+ showed a preference for the coherent motion, though in a different degree, area V3A showed the opposite pattern, being more activated in the random condition (see N180 component). This result is unexpected because it is in contrast with previous works on humans reporting that %BOLD signal change in V3A was greater for coherent than for random motion (Braddick et al., 2000, 2001; Moutoussis et al., 2005; Vaina et al., 2003). Moreover, several studies have shown that V3A is responsive to flow-fields stimulation (e.g., Helfrich et al., in press; Pitzalis et al., 2010; Sereno et al., 2001) and to other types of global motion signals, as those involved in reconstruction of form from motion (Orban et al., 1999). Although in contrast with the other human data, result found here relates directly to macaque physiology. Indeed, it has been assumed that large receptive fields are needed to encode coherent motion (e.g., Duffy, 1998; Duffy and Wurtz, 1991a), and the receptive fields in V3A are much smaller than those in motion areas as MT and MST (Desimone and Ungerleider, 1986; Galletti and Battaglini, 1989; Komatsu and Wurtz, 1988), areas which are typically involved in coherent motion analysis. The large stimuli used here presumably exceeded the small receptive field size of neurons in area V3A and did not allow for sufficient summation within the receptive fields (see also Becker et al., 2008 for similar data interpretation). However, caution is required in data interpretation, because the effects (in terms of signal difference between coherent and incoherent motion) are small and the uncertainty about the level of baseline in fMRI studies is high. Further studies testing coherent motion along with other cardinal dimensions (i.e., translational, circular etc.) are needed to verify this point.

Parallel signal flow from the occipital pole to the medial and lateral motion areas V6 and MT+

The lateral area MT+ (e.g. Wall and Smith, 2008) and the medial area V6 (Cardin and Smith, 2010; Pitzalis et al., 2010) are considered key motion areas within the human dorsal visual stream. Our analyses show a rapid sequence of activation from the occipital pole to these two motion areas of the dorsal stream. MT+ and V6 have similar onset latencies (100 and 105 ms), with a delay of about 25 ms with respect to V1 peak, and both showed a preference for the coherent motion. The minimal temporal gap between the two areas supports the view of direct interconnections between V1 and the two motion areas, as found in the macaque brain (Galletti et al., 2001; Shipp and Zeki, 1989) and suggests that that the flow sensitivity in V6 is not inherited from MT+ but constructed de novo from V1 afferents. Also previous MEG studies found visual activity in POS and V1 in a similar latency range (Vanni et al., 2001; von Pföstl et al., 2009). However, in those studies, the response onset of a temporo-occipital region (likely corresponding to MT/V5) was significantly (about 20 ms) delayed with respect to POS no matter whether static or moving stimuli were used. Present data do not support those results. Here we found the earliest activity in V1 and then, almost simultaneously, in MT+ and V6. In this respect our data are more similar to those reported in a earlier MEG study which found no significant differences between the onset latencies of the POS and the temporal occipital (TO) region, which likely includes the motion sensitive MT+ (Tzelepi et al., 2001).

Our results suggest that motion signals flow in parallel from the occipital pole to the medial and lateral motion areas V6 and MT+. These two areas likely exchange information on visual motion, as it is the case in the macaque monkey (Galletti et al., 2001), even though the present data do not represent a direct evidence of connections between them. Since it is unlikely that two cortical areas do the same job in the brain, the question is: which is the differential role of V6 and MT+ on a functional point of view? It is now clear that the two motion areas have different patterns of anatomical connectivity: V6 is only connected with areas of the dorsal visual stream (Galletti et al., 2001), mainly located in the SPL, whereas V5/MT with cortical areas located in the inferior parietal lobule, and with areas of the ventral visual stream (Boussaoud et al., 1990). On the functional point of view, V5/MT is involved in the analysis of motion signals (direction and speed of movement) particularly in the central part of the visual field, whereas V6 in both object and self-motion recognition across the whole visual field (see Galletti and Fattori, 2003). The hypothesis that V6 is involved in object and self-motion recognition is based on the fact that it contains many "real-motion cells," that is, cells activated by the actual movement of an object in the visual field regardless of the movement of object retinal image induced by the eye movements (Galletti and Fattori, 2003). In a previous MEG study in humans, Tikhonov et al. (2004) compared MEG responses under two conditions of retinal image motion which were physically identical but gave rise to different percepts of visual motion. They demonstrated that the perception of self-induced visual motion resides in the medial aspect of the parieto-occipital cortex, a region that likely includes area V6. Given the high incidence of real-motion cells in V6 and the fact that V6 uniformly represents the whole visual field up to the far periphery, we believe that, as suggested in a previous work (Pitzalis et al., 2010), V6 is involved in 'subtracting out' self motion signals across the whole visual field.

From V6, visual information would then reach bimodal visual/somatosensory areas in the superior parietal lobule (areas V6A and MIP) that are able to encode visual space and arm reaching movement (Colby and Duhamel, 1991; Galletti and Fattori, 2002; Galletti et al., 2001, 2003). Thus, even though area V6 is not directly involved in the control of arm movement, the ability of V6 cells to recognize the "real movement" in the visual field and to encode the direction of movement of objects could be useful to encode the continuously changing spatial location of moving objects, providing the spatial coordinates of moving targets to the controllers of arm reaching movements. Future studies using functional connectivity analysis of fMRI data will be needed to verify the proposed model.

Acknowledgments

We thank Dr. Stefano Sdoia for helping with figures. This research was supported by grants from the University of Rome "Foro Italico" to SP and FDR, the Italian Ministry of University and Research, and the Fondazione del Monte di Bologna e Ravenna, Italy to CG and PF.

References

Becker, H.G., Erb, M., Haarmeier, T., 2008. Differential dependency on motion coherence in subregions of the human MT+ complex. Eur. J. Neurosci. 28 (8), 1674–1685.
Bocker, K.B.E., Cornelis, H.M., Brunia, C.H.M., Van den Berg-Lenss, M.M.C., 1994. A spatiotemporal dipole model of the stimulus preceding negativity prior to feedback stimuli. Brain Topogr. 7, 71–88.
Boussaoud, D., Ungerleider, L.G., Desimone, R., 1990. Pathways for motion analysis: cortical connections of the medial superior temporal and fundus of the superior temporal visual areas in the macaque. J. Comp. Neurol. 296, 462–495.
Braddick, O.J., O'Brien, J.M., Wattam-Bell, J., Atkinson, J., Turner, R., 2000. Form and motion coherence activate independent, but not dorsal/ventral segregated, networks in the human brain. Curr. Biol. 10 (12), 731–734.
Braddick, O.J., O'Brien, J.M., Wattam-Bell, J., Atkinson, J., Hartley, T., Turner, R., 2001. Brain areas sensitive to coherent visual motion. Perception 30 (1), 61–72.
Bremmer, F., Schlack, A., Shah, N.J., Zafiris, O., Kubischik, M., Hoffmann, K.P., Zilles, K., Fink, G.R., 2001. Polymodal motion processing in posterior parietal and premotor cortex. Neuron 29 (1), 287–296.
Cardin, V., Smith, A.T., 2010. Sensitivity of human visual and vestibular cortical regions to egomotion-compatible visual stimulation. Cereb. Cortex 20 (8), 1964–1973.
Cardin, V., Smith, A.T., 2011. Sensitivity of human visual cortical area V6 to stereoscopic depth gradients associated with self-motion. J. Neurophysiol. 106 (3), 1240–1249.
Castriota-Scanderbeg, A., Hagberg, G.E., Cerasa, A., Committeri, G., Galati, G., Patria, F., Pitzalis, S., Caltagirone, C., Frackowiak, R., 2005. The appreciation of wine by sommeliers: a functional magnetic resonance study of sensory integration. NeuroImage 25, 570–578.
Clark, V.P., Fan, S., Hillyard, S.A., 1995. Identification of early visually evoked potential generators by retinotopic and topographic analysis. Hum. Brain Mapp. 2, 170–187.
Colby, C.L., Duhamel, J.R., 1991. Heterogeneity of extrastriate visual areas and multiple parietal areas in the macaque monkey. Neuropsychologia 29 (6), 517–537.
Dale, A.M., Fischl, B., Sereno, M.I., 1999. Cortical surface-based analysis. I. Segmentation and surface reconstruction. NeuroImage 9, 179–194.
Desimone, R., Ungerleider, L.G., 1986. Multiple visual areas in the caudal superior temporal sulcus of the macaque. J. Comp. Neurol. 248 (2), 164–189.
Di Russo, F., Martínez, A., Sereno, M.I., Pitzalis, S., Hillyard, S.A., 2002. The cortical sources of the early components of the visual evoked potential. Hum. Brain Mapp. 15, 95–111.
Di Russo, F., Martínez, A., Hillyard, S.A., 2003. Source analysis of event-related cortical activity during visuo-spatial attention. Cereb. Cortex 13, 486–499.
Di Russo, F., Pitzalis, S., Spitoni, G., Aprile, T., Patria, F., Spinelli, D., Hillyard, S.A., 2005. Identification of the neural sources of the pattern-reversal VEP. NeuroImage 24, 874–886.
Di Russo, F., Pitzalis, S., Aprile, T., Spitoni, G., Patria, F., Stella, A., Spinelli, D., Hillyard, S.A., 2007. Spatio-temporal analysis of the cortical sources of the steady-state visual evoked potential. Hum. Brain Mapp. 28, 323–334.
Di Russo, F., Stella, A., Spitoni, G., Strappini, F., Sdoia, S., Galati, G., Hillyard, S.A., Spinelli, D., Pitzalis, S., 2011. Spatiotemporal brain mapping of spatial attention effects on pattern-reversal ERPs. Hum. Brain Mapp. 33 (6), 1334–1351.
Duffy, C.J., 1998. MST neurons respond to optic flow and translational movement. J. Neurophysiol. 80 (4), 1816–1827.
Duffy, C.J., Wurtz, R.H., 1991a. Sensitivity of MST neurons to optic flow stimuli. I. A continuum of response selectivity to large-field stimuli. J. Neurophysiol. 65 (6), 1329–1345.
Duffy, C.J., Wurtz, R.H., 1991b. Sensitivity of MST neurons to optic flow stimuli. II. Mechanisms of response selectivity revealed by small-field stimuli. J. Neurophysiol. 65 (6), 1346–1359.
Duffy, C.J., Wurtz, R.H., 1995. Response of monkey MST neurons to optic flow stimuli with shifted centers of motion. J. Neurosci. 15 (7 Pt 2), 5192–5208.
Fischer, E., Bülthoff, H.H., Logothetis, N.K., Bartels, A., 2012. Visual motion responses in the posterior cingulate sulcus: a comparison to V5/MT and MST. Cereb. Cortex 22 (4), 865–876.
Fischl, B., Sereno, M.I., Dale, A.M., 1999. Cortical surface-based analysis. II. Inflation, flattening, and a surface-based coordinate system. NeuroImage 9, 195–207.
Friston, K.J., Ashburner, J., Poline, J.B., Frith, C.D., Heather, J.D., Frackowiak, R.S.J., 1995. Spatial registration and normalization of images. Hum. Brain Mapp. 2, 165–189.
Galati, G., Committeri, G., Spitoni, G., Aprile, T., Di Russo, F., Pitzalis, S., Pizzamiglio, L., 2008. A selective representation of the meaning of actions in the auditory mirror system. NeuroImage 40, 1274–1286.
Galati, G., Committeri, G., Pitzalis, S., Pelle, G., Patria, F., Fattori, P., Galletti, C., 2011. Intentional signals during saccadic and reaching delays in the human posterior parietal cortex. Eur. J. Neurosci. 34 (11), 1871–1885.
Galletti, C., Battaglini, P.P., 1989. Gaze-dependent visual neurons in area V3A of monkey prestriate cortex. J. Neurosci. 9, 1112–1125.
Galletti, C., Fattori, P., 2002. Posterior parietal networks encoding visual space. In: Karnath, H.O., Milner, A.D., Vallar, G. (Eds.), The Cognitive and Neural Bases of Spatial Neglect. Oxford University Press, Oxford, New York, pp. 59–69 (ISBN 0 19 850833 6 Hbk).
Galletti, C., Fattori, P., 2003. Neuronal mechanisms for detection of motion in the field of view. Neuropsychologia 41, 1717–1727.
Galletti, C., Battaglini, P.P., Fattori, P., 1990. 'Real-motion' cells in area V3A of macaque visual cortex. Exp. Brain Res. 82, 67–76.
Galletti, C., Fattori, P., Gamberini, M., Kutz, D.F., 1999. The cortical visual area V6: brain location and visual topography. Eur. J. Neurosci. 11, 3922–3936.
Galletti, C., Gamberini, M., Kutz, D.F., 2001. The cortical connections of area V6: an occipito-parietal network processing visual information. Eur. J. Neurosci. 13, 1572–1588.
Galletti, C., Kutz, D., Gamberini, M., Breveglieri, R., Fattori, P., 2003. Role of the medial parieto-occipital cortex in the control of reaching and grasping movements. Exp. Brain Res. 153, 158–170.
Hagler Jr., D.J., Sereno, M.I., 2006. Spatial maps in frontal and prefrontal cortex. NeuroImage 29, 567–577.
Helfrich, R.F., Becker, H.G., Haarmeier, T., in press. Processing of coherent visual motion in topographically organized visual areas in human cerebral cortex. Brain Topogr. http://dx.doi.org/10.1007/s10548-012-0226-1.
Hoffmann, M.B., Bach, M., 2002. The distinction between eye and object motion is reflected by the motion-onset visual evoked potential. Exp. Brain Res. 144, 141–151.
Holliday, I.E., Meese, T.S., 2005. Neuromagnetic evoked responses to complex motions are greatest for expansion. Int. J. Psychophysiol. 55 (2), 145–157.
Huk, A.C., Dougherty, R.F., Heeger, D.J., 2002. Retinotopy and functional subdivision of human areas MT and MST. J. Neurosci. 22, 7195–7205.
Ionta, S., Heydrich, L., Lenggenhager, B., Mouthon, M., Fornari, E., Chapuis, D., Gassert, R., Blanke, O., 2011. Multisensory mechanisms in temporoparietal cortex support self-location and first-person perspective. Neuron 70, 363–374.
Jeffreys, D.A., Axford, J.G., 1972. Source locations of pattern-specific component of human visual evoked potentials. I. Component of striate cortical origin. Exp. Brain Res. 16 (1), 1–21.
Kolster, H., Peeters, R., Orban, G.A., 2010. The retinotopic organization of the human middle temporal area MT/V5 and its cortical neighbors. J. Neurosci. 30 (29), 9801–9820.
Komatsu, H., Wurtz, R.H., 1988. Relation of cortical areas MT and MST to pursuit eye movements. III. Interaction with full-field visual stimulation. J. Neurophysiol. 60 (2), 621–644.
Konen, C.S., Kastner, S., 2008. Representation of eye movements and stimulus motion in topographically organized areas of human posterior parietal cortex. J. Neurosci. 28 (33), 8361–8375.
Kovács, G., Raabe, M., Greenlee, M.W., 2008. Neural correlates of visually induced self-motion illusion in depth. Cereb. Cortex 18, 1779–1787.
Kremlácek, J., Kuba, M., Chlubnová, J., Kubová, Z., 2004. Effect of stimulus localisation on motion-onset VEP. Vis. Res. 44, 2989–3000.
Kuba, M., Kubová, Z., Kremlábek, J., Langrová, J., 2007. Motion-onset VEPs: characteristics, methods, and diagnostic use. Vis. Res. 47, 189–202.
Kwong, K.K., Belliveau, J.W., Chesler, D.A., Goldberg, I.E., Weisskoff, R.M., Poncelet, B.P., Kennedy, D.N., Hoppel, B.E., Cohen, M.S., Turner, R., Cheng, H.M., Brady, T.J., Rosen, B.R., 1992. Dynamic magnetic resonance imaging of human brain activity during primary sensory stimulation. Proc. Natl. Acad. Sci. U. S. A. 89 (12), 5675–5679.
Lancaster, J.L., Woldorff, M.G., Parsons, L.M., Liotti, M., Freitas, C.S., Rainey, L., Kochunov, P.V., Nickerson, D., Mikiten, S.A., Fox, P.T., 2000. Automated Talairach atlas labels for functional brain mapping. Hum. Brain Mapp. 10 (3), 120–131.
Larsson, J., Heeger, D.J., 2006. Two retinotopic visual areas in human lateral occipital cortex. J. Neurosci. 26, 13128–13142.
Lebranchu, P., Bastin, J., Pelegrini-Issac, M., Lehericy, S., Berthoz, A., Orban, G.A., 2010. Retinotopic coding of extraretinal pursuit signals in early visual cortex. Cereb. Cortex 20 (9), 2172–2187.
Mazziotta, J.C., Toga, A.W., Evans, A., Fox, P., Lancaster, J., 1995. A probabilistic atlas of the human brain: theory and rationale for its development. The International Consortium for Brain Mapping (ICBM). NeuroImage 2, 89–101.
McKeefry, D.J., Burton, M.P., Vakrou, C., Barrett, B.T., Morland, A.B., 2008. Induced deficits in speed perception by transcranial magnetic stimulation of human cortical areas V5/MT+ and V3A. J. Neurosci. 28, 6848–6857.
Mercier, M., Schwartz, S., Michel, C.M., Blanke, O., 2009. Motion direction tuning in human visual cortex. Eur. J. Neurosci. 29 (2), 424–434.
Morrone, M.C., Tosetti, M., Fiorentini, A., Cioni, G., Burr, D.C., 2000. A cortical area that responds specifically to optic flow, revealed by fMRI. Nat. Neurosci. 3, 1322–1328.
Moutoussis, K., Keliris, G., Kourtzi, Z., Logothetis, N., 2005. A binocular rivalry study of motion perception in the human brain. Vis. Res. 45 (17), 2231–2243.
Orban, G.A., Sunaert, S., Todd, J.T., van Hecke, P., Marchal, G., 1999. Human cortical regions involved in extracting depth from motion. Neuron 24, 929–940.
Orban, G.A., Fize, D., Peuskens, H., Denys, K., Nelissen, K., Sunaert, S., Todd, J., Vanduffel, W., 2003. Similarities and differences in motion processing between the human and macaque brain: evidence from fMRI. Neuropsychologia 41 (13), 1757–1768.
Pitts, M.A., Martínez, A., Hillyard, S.A., 2010. When and where is binocular rivalry resolved in the visual cortex? J. Vis. 10 (14), 25.
Pitzalis, S., Galletti, C., Huang, R.S., Patria, F., Committeri, G., Galati, G., Fattori, P., Sereno, M.I., 2006. Wide-field retinotopy defines human cortical visual area V6. J. Neurosci. 26, 7962–7973.
Pitzalis, S., Sereno, M.I., Committeri, G., Fattori, P., Galati, G., Patria, F., Galletti, C., 2010. Human V6: the medial motion area. Cereb. Cortex 20 (2), 411–424.
Pitzalis, S., Strappini, F., De Gasperis, M., Bultrini, A., Di Russo, F., 2012. Spatio-temporal brain mapping of motion-onset VEPs combined with fMRI and retinotopic maps. PLoS One 7 (4), e35771.
Previc, F.H., Liotti, M., Blakemore, C., Beer, J., Fox, P., 2000. Functional imaging of brain areas involved in the processing of coherent and incoherent wide field-of-view visual motion. Exp. Brain Res. 131 (4), 393–405.
Saito, H., Yukie, M., Tanaka, K., Hikosaka, K., Fukada, Y., Iwai, E., 1986. Integration of direction signals of image motion in the superior temporal sulcus of the macaque monkey. J. Neurosci. 6 (1), 145–157.

Sdoia, S., Pitzalis, S., Bultrini, A., Di Russo, F., Fattori, P., Galati, G., Galletti, C., 2009. Sensitivity to optic flow components in human cortical area V6 and other cortical motion areas. NeuroImage 47, S86.
Sereno, M.I., Huang, R.-S., 2006. A human parietal face area contains aligned head-centered visual and tactile maps. Nat. Neurosci. 9, 1337–1343.
Sereno, M.I., Dale, A.M., Reppas, J.B., Kwong, K.K., Belliveau, J.W., Brady, T.J., Rosen, B.R., Tootell, R.B., 1995. Borders of multiple visual areas in humans revealed by functional magnetic resonance imaging. Science 268, 889–893.
Sereno, M.I., Pitzalis, S., Martinez, A., 2001. Mapping of contralateral space in retinotopic coordinates by a parietal cortical area in humans. Science 294, 1350–1354.
Shipp, S., Zeki, S., 1989. The organization of connections between areas V5 and V1 in macaque monkey visual cortex. Eur. J. Neurosci. 1, 309–332.
Silver, M.A., Ress, D., Heeger, D.J., 2005. Topographic maps of visual spatial attention in human parietal cortex. J. Neurophysiol. 94, 1358–1371.
Smith, A.T., Greenlee, M.W., Singh, K.D., Kraemer, F.M., Hennig, J., 1998. The processing of first- and second-order motion in human visual cortex assessed by functional magnetic resonance imaging (fMRI). J. Neurosci. 18, 3816–3830.
Smith, T., Wall, M.B., Williams, A.L., Singh, K.D., 2006. Sensitivity to optic flow in human cortical areas MT and MST. Eur. J. Neurosci. 23, 561–569.
Smith, A.T., Wall, M.B., Thilo, K.V., 2012. Vestibular inputs to human motion-sensitive visual cortex. Cereb. Cortex 22 (5), 1068–1077.
Sunaert, S., Van Hecke, P., Marchal, G., Orban, G.A., 1999. Motion-responsive regions of the human brain. Exp. Brain Res. 127 (4), 355–370.
Swisher, J.D., Halko, M.A., Merabet, L.B., McMains, S.A., Somers, D.C., 2007. Visual topography of human intraparietal sulcus. J. Neurosci. 27, 5326–5337.
Talairach, J., Tournoux, P., 1988. Co-planar Stereotaxic Atlas of the Human Brain. Thieme, New York.
Tikhonov, A., Haarmeier, T., Their, P., Braun, C., Lutzenberger, W., 2004. Neuromagnetic activity in medial parietooccipital cortex reflects the perception of visual motion during eye movements. NeuroImage 21, 593–600.
Tootell, R.B., Hadjikhani, N., 2001. Where is 'dorsal V4' in human visual cortex? Retinotopic, topographic and functional evidence. Cereb. Cortex 11, 298–311.
Tootell, R.B., Reppas, J.B., Kwong, K.K., Malach, R., Born, R.T., Brady, T.J., Rosen, B.R., Belliveau, J.W., 1995. Functional analysis of human MT and related visual cortical areas using magnetic resonance imaging. J. Neurosci. 1, 3215–3230.
Tootell, R.B., Mendola, J.D., Hadjikhani, N.K., Ledden, P.J., Liu, A.K., Reppas, J.B., Sereno, M.I., Dale, A.M., 1997. Functional analysis of V3A and related areas in human visual cortex. J. Neurosci. 17, 7076–7078.
Tzelepi, A., Ioannides, A.A., Poghosyan, V., 2001. Early (N70m) neuromagnetic signal topography and striate and extrastriate generators following pattern onset quadrant stimulation. NeuroImage 13 (4), 702–718.
Tzourio-Mazoyer, N., Landeau, B., Papathanassiou, D., Crivello, F., Etard, O., Delcroix, N., Mazoyer, B., Joliot, M., 2002. Automated anatomical labeling of activations in SPM using a macroscopic anatomical parcellation of the MNI MRI single-subject brain. NeuroImage 15 (1), 273–289.
Urakawa, T., Inui, K., Kakigi, R., 2010. Effects of stimulus field size and coherence of visual motion on cortical responses in humans: an MEG study. Neurosci. Lett. 488 (3), 294–298.
Vaina, L.M., Gryzwacz, N.M., Saiviroonporn, P., LeMay, M., Bienfang, D.C., Cowey, A., 2003. Can spatial and temporal motion integration compensate for deficits in local motion mechanisms? Neuropsychologia 41 (13), 1817–1836.
Van Essen, D.C., 2005. A population-average, landmark- and surface-based (PALS) atlas of human cerebral cortex. NeuroImage 28 (3), 635–662.
Van Oostende, S., Sunaert, S., Van Hecke, P., Marchal, G., Orban, G.A., 1997. The kinetic occipital (KO) region in man: an fMRI study. Cereb. Cortex 7, 690–701.
Vanduffel, W., Fize, D., Peuskens, H., Denys, K., Sunaert, S., Todd, J.T., Orban, G.A., 2002. Extracting 3D from motion: differences in human and monkey intraparietal cortex. Science 298 (5592), 413–415.
Vanni, S., Tanskanen, T., Seppa, M., Uutela, K., Hari, R., 2001. Coinciding early activation of the human primary visual cortex and anteromedial cuneus. Proc. Natl. Acad. Sci. U. S. A. 98 (5), 2776–2780.
von Pföstl, V., Stenbacka, L., Vanni, S., Parkkonen, L., Galletti, C., Fattori, P., 2009. Motion sensitivity of human V6: a magnetoencephalography study. NeuroImage 45 (4), 1253–1263.
Wall, M.B., Smith, A.T., 2008. The representation of egomotion in the human brain. Curr. Biol. 18, 191–194.
Wall, M.B., Lingnau, A., Ashida, H., Smith, A.T., 2008. Selective visual responses to expansion and rotation in the human MT complex revealed by functional magnetic resonance imaging adaptation. Eur. J. Neurosci. 27, 2747–2757.
Watson, J.D., Myers, R., Frackowiak, R.S., Hajnal, J.V., Woods, R.P., Mazziotta, J.C., Shipp, S., Zeki, S., 1993. Area V5 of the human brain: evidence from a combined study using positron emission Tomography and magnetic resonance imaging. Cereb. Cortex 3, 79–94.
Wiest, G., Amorim, M.A., Mayer, D., Schick, S., Deecke, L., Lang, W., 2001. Cortical responses to object-motion and visually-induced self-motion perception. Brain Res. Cogn. Brain Res. 12 (1), 167–170.
Zeki, S.M., 1978. The third visual complex of rhesus monkey prestriate cortex. J. Physiol. (Lond.) 277, 245–272.
Zeki, S., Watson, J.D.G., Lueck, C.J., Friston, K.J., Kennard, C., Frackowiak, R.S.J., 1991. A direct demonstration of functional specialization in the human visual cortex. J. Neurosci. 11, 641–649.
Zhang, X., Zhaoping, L., Zhou, T., Fang, F., 2012. Neural activities in V1 create a bottom-up saliency map. Neuron 73 (1), 183–192.